How to cite: *Angew. Chem. Int. Ed.* **2020**, *59*, 20672 – 20681
International Edition: doi.org/10.1002/anie.202009648
German Edition: doi.org/10.1002/ange.202009648

Molecular Sieves

Water-Induced Structural Dynamic Process in Molecular Sieves under Mild Hydrothermal Conditions: Ship-in-a-Bottle Strategy for Acidity Identification and Catalyst Modification

Tantan Sun, Shutao Xu, Dong Xiao, Zhiqiang Liu, Guangchao Li, Anmin Zheng, Wenjuan Liu, Zhaochao Xu, Yi Cao, Qiang Guo, Nan Wang, Yingxu Wei,* and Zhongmin Liu**

Abstract: *Water is the most important substance in nature. Imitating the formation of natural materials, molecular sieves have been synthesized under hydrothermal conditions and applied in industry. Herein, we reveal an unforeseen observation on a very special water-induced structural dynamic process of these materials. Dynamic and reversible breaking and forming of T-O-T bonds in silicoaluminophosphate (SAPO) occurs through interactions between gaseous water and the molecular-sieve framework under mild hydrothermal conditions and is confirmed by detection of the incorporation of ^{17}O from $H_2{}^{17}O$ into molecular-sieve framework. Encapsulation of the bulky molecules trimethylphosphine and pyridine (kinetic diameters much larger than the pore size of SAPO-34) into CHA cavities consolidated the water-induced dynamic process. Consequently, new insights into the dynamic features of molecular sieves in water are provided. The ship-in-a-bottle strategy based on these findings also open new fields for fine acidity identification and gives extra boost in shape-selective catalysis.*

Introduction

Water is the source of all things and the foundation of life in the earth. Water not only participates in important life processes, it is also the most ideal medium for many physical, chemical, and biological processes that we have discovered, invented and developed.[1–4] The participation and role of water in these processes is enduring and important subjects that people have been pursuing. As a result, a large number of scientific research achievements in applied materials and industrial processes have been developed in the fields of science and technology.[5–8] Catalysis is a key pillar of the energy industry and zeolites or molecular sieves are widely used in industrial processes. Up to now, more than 250 topologies of molecular sieves with compositional variability have been synthesized under hydrothermal condition with the participation of water at a certain temperature and pressure.[9–11] Based on the specific crystal structures and unique porosity, molecular sieves are extensively-used as sorbents, ion exchangers, separating agents, sensors, drug deliverers, and in particular, catalysts in industrial processes, and well-acknowledged as the most significant groups in the class of porous materials.[9,12–14]

In the hydrothermal synthesis process of molecular sieves, starting materials, such as amorphous gels, are depolymerized to form soluble aluminates and silicates that composed of the building units firstly.[15] Then these units can be further repolymerized at certain hydrothermal conditions, thus crystallographic structures with various topologies are constructed under the guidance of structure-directing agents eventually.[9,10,15,16] This process includes two critical steps: (1) the generation of the building units and (2) the self-assembly of these units. Water is an essential substance for the successful synthesis and has the following functions: working as reaction medium, determining the extent of hydrolysis, accelerating the condensation reactions and modulating the crystallization kinetics.[17–19] Besides the necessity for hydrothermal synthesis, water vapor or steam also play a significant role in post-treatment for molecular sieves modification. High-temperature (> 600 °C) steaming is often used for

[*] Dr. T. Sun, Prof. S. Xu, Dr. Y. Cao, Dr. Q. Guo, Dr. N. Wang, Prof. Y. Wei, Prof. Z. Liu
National Engineering Laboratory for Methanol to Olefins, Dalian National Laboratory for Clean Energy, iChEM (Collaborative Innovation Center of Chemistry for Energy Materials), Dalian Institute of Chemical Physics, Chinese Academy of Sciences
Dalian 116023 (China)
E-mail: xushutao@dicp.ac.cn
weiyx@dicp.ac.cn
liuzm@dicp.ac.cn

Dr. D. Xiao, Prof. Z. Liu
State Key Laboratory of Catalysis, Dalian Institute of Chemical Physics, Chinese Academy of Sciences
Dalian 116023 (China)

Dr. Z. Liu, Dr. G. Li, Prof. A. Zheng, Prof. Z. Liu
State Key Laboratory of Magnetic Resonance and Atomic and Molecular Physics, National Center for Magnetic Resonance in Wuhan, Wuhan Institute of Physics and Mathematics, Innovation Academy for Precision Measurement Science and Technology, Chinese Academy of Sciences
Wuhan 430071 (China)

Dr. W. Liu, Prof. Z. Xu
Key Laboratory of Separation Science for Analytical Chemistry, Dalian Institute of Chemical Physics, Chinese Academy of Sciences
Dalian 116023 (China)

Dr. T. Sun, Dr. G. Li, Dr. W. Liu, Dr. N. Wang
University of Chinese Academy of Sciences
Beijing 100049 (China)

Supporting information and the ORCID identification number(s) for the author(s) of this article can be found under: https://doi.org/10.1002/anie.202009648.

dealumination to construct hierarchical porosity, reduce acid density and improve the hydrothermal stability of molecular sieves (Scheme 1 a).[20–22] For example, the ultra-stable Y (USY) zeolite with higher Si/Al ratio, widely-used in fluid-catalytic-cracking (FCC) process, is typically obtained by dealumination via high-temperature hydrothermal treatment.[23,24] Meanwhile, low-temperature (usually $<100\,^{\circ}C$) steaming can also exert profound influence on molecular-sieve framework. The adsorption of water at low-temperature strongly influences the crystallinity, acidity and adsorption sites of molecular sieves[25–27] which leads to the hydrated hydronium cluster ions $H_3O^+.(H_2O)_n$[25,26] and penta/hexa-coordinated P or Al species.[28] Recently, studies by Morris and Ashbrook et al. found the molecular-sieve framework can be even hydrolyzed when in contact with water at room-temperature.[29,30] What about the molecular sieves in the water vapor atmosphere at the moderate-temperature range from 100 to 500 °C, the very important condition for heterogeneous catalytic reactions to occur. In the industrial processes (mainly performed at 100–500 °C) using zeolite/SAPO-catalysts, co-fed or co-produced water not only acts as diluter for lowering the partial pressure of reactants and removing heat from reactor, but also can compete with reactants in accessing the active sites to slow down the reaction and prolong the catalyst lifetime by reducing the coking.[31,32] Even the hydrothermal circumstance, the molecular-sieve framework is generally considered to be hydrothermally stable and unaffected by water at this temperature range, since no

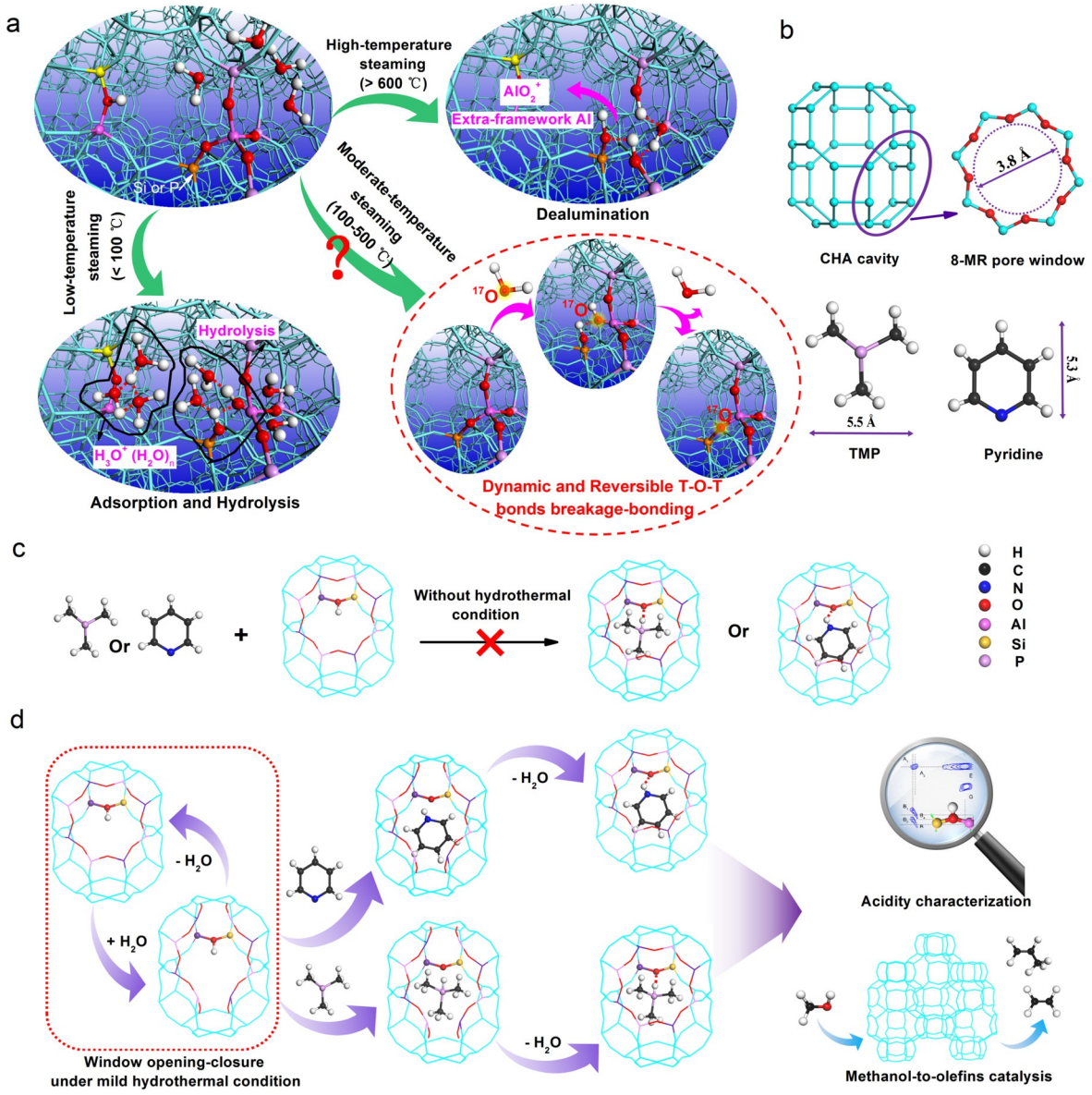

Scheme 1. a) Interactions between water and molecular-sieve framework at different steaming conditions. b) Topology of SAPO-34 with CHA cavity and 8-MR window with diameter of 3.8 Å, and the steric configuration of TMP and pyridine molecules with kinetic diameters of 5.5 Å and 5.3 Å respectively. c) The impossibility of encapsulating TMP and pyridine into CHA cavities without the aid of hydrothermal conditions. d) The encapsulation strategy of TMP and pyridine into CHA cavities under mild hydrothermal conditions and their further applications for acidity characterization and catalyst modification.

obvious loss of crystallinity and acidity occur and even no water adsorption is observed during the reactions.[9,31,33]

Some important zeolites and SAPO molecular sieves usually work in the environment of water vapor atmosphere at elevated temperature when they are applied in petrochemical or coal chemical industry. In the catalytic petroleum refining, the zeolite catalysts, such as Pt/MOR, ZSM-5, ZSM-22 and Y, are exposed in a harsh hydrothermal environment since steam is commonly used as the driving gas in the hydroisomerization, hydrocracking and FCC operations.[24,34] Additionally, SAPO-34 molecular sieve with CHA topology that featured as narrow 8-MR window (3.8 Å × 3.8 Å) and super-cage structure (Scheme 1 b), has been successfully applied in industrial methanol-to-olefins (MTO) and selective-catalytic-reduction (SCR) of nitrogen oxides (NO_x) processes in which water is co-fed and co-produced substance.[35–38] However, at the temperature range for catalytic processes, due to the lack of suitable research techniques that reflect the attack from water on the zeolite/SAPO-catalysts, the effects of hydrothermal conditions on the molecular-sieve framework, which are critical for a deeply understanding of the functions of water during catalytic reaction, have not yet been studied. In this work, a surprising dynamic and reversible breaking and forming of T-O-T bonds in SAPO-34 molecular sieve under mild hydrothermal conditions (100–300 °C) was successfully revealed by employing ^{17}O-labelled water ($H_2{}^{17}O$) for moderate-temperature steaming and the incorporation of ^{17}O atoms from $H_2{}^{17}O$ into the molecular-sieve framework was captured. We demonstrated that the T-O-T bonds breaking and forming is dynamic and reversible, leading to the fast 8-MR pore opening-closure of SAPO-34. Two bulky probe molecules trimethylphosphine (TMP) and pyridine with kinetic diameters 5.5 Å and 5.3 Å respectively (much larger than the 8-MR pore size (3.8 Å) of SAPO-34, Scheme 1 b)[39,40] are successfully encapsulated into CHA cavities of SAPO-34 by the aid of hydrothermal conditions (Scheme 1 c,d). This unusual encapsulation not only consolidated the dynamic and reversible breaking and forming of T-O-T bonds, but also brought very special applications in acid characterization and shape-selective catalysis.

Results and Discussion

Dynamic and reversible T-O-T bonds breaking and forming in SAPO molecular sieve under mild hydrothermal conditions

To present real-time dynamic changes of molecular-sieve framework under hydrothermal conditions, in situ solid-state NMR measurements of the continuous-flow steam treatment for SAPO-34 (synthesized by the hydrothermal method in Supporting Information and the SEM image was shown in Figure S1) were conducted in a rotor at 300 °C. As shown in Figure S2, the time-resolved ^{31}P and ^{27}Al MAS NMR spectra exhibit the solitary signal that belongs to framework tetrahedral P and Al species at −29.5 and 38 ppm, respectively, and these spectra show no differences during steaming from 0 to 120 min. These in situ observations may stem from two possibilities: (1) water may have no effects on molecular-sieve framework due to weak adsorption under this hydrothermal condition, and (2) the resulted variations under this hydrothermal condition for molecular-sieve framework is in a very fast process that cannot be captured by in situ solid-state NMR spectroscopy. In fact, both the weak adsorption of water and the fast processes related to hydrothermal effects have not been revealed yet, due to the great difficulty or even impossibility in the confirmation of these behaviors. Although the removal of framework elements and structural damages by high-temperature steaming[21] and the framework stability at low-temperature[41] have been extensively reported. Directly evidencing the variations of molecular-sieve framework under the hydrothermal conditions close to the catalytic reactions is still a huge challenge due to the limitation of current experimental techniques.

To further clarify the specific functions of water under mild hydrothermal conditions on molecular-sieve framework, exploratory usage of $H_2{}^{17}O$ to interact with SAPO-34 molecular sieve was attempted at the temperature range of 100–300 °C (see Experimental Section in Supporting Information) and the achieved steam-treated samples were measured by ^{17}O MAS NMR spectroscopy. Surprisingly, the ^{17}O MAS NMR spectra exhibited in Figure 1 a clearly demonstrate two broad resonance signals at 21 and 48 ppm, attributing to the framework ^{17}O atoms in the Si-O-Al and P-O-Al species as the linking oxygen confirmed by 2D ^{17}O MQMAS spectrum (Figure 1 b).[29,42,43] These unexpected results imply that ^{17}O atoms from $H_2{}^{17}O$ are incorporated into molecular-sieve framework, suggesting that part of the tetrahedrally coordinated structure of SAPO-34 may undergo a dynamic T-O-T bonds breaking by hydrolysis when interacting with water vapor, but in a following step, dehydration reaction completely recovers the framework immediately. After this dynamic procedure, no terminal hydroxy groups are newly generated and the crystallinity remained unchanged, comparing with the untreated sample (Figure 1 c, Figure S3 and S4), while the incorporated and retained ^{17}O atoms on the steamed SAPO-34 reveal the reversible hydration-dehydration process (Figure 1 d). Considering the observation failure of T-O-T bonds changes by in situ solid-state NMR spectroscopy, it can be inferred that this dynamic and reversible process involving of hydrolysis-dehydration step is a very fast process beyond the time resolution of in situ NMR technique. Generally, the framework of molecular sieves was considered to be less affected by water and the hydrothermal stability can be well-kept at moderate-temperature based on the weak adsorption of water and the unchanged crystallinity after dehydration. In very recent study, Kalantzopoulos et al. found that the framework of molecular sieves become labile with subtle changes of T atoms when interacting with water at 250–300 °C.[44] In the present work, a water-induced dynamic and reversible process of breaking and forming of T-O-T bonds is directly and definitely confirmed by using $H_2{}^{17}O$ for hydrothermal treatment. Moreover, as evidenced in Figure 1 a, the breaking and forming of T-O-T bonds becomes more easily to be realized in the $H_2{}^{17}O$ atmosphere at enhanced temperature, as is indicated that more ^{17}O atoms from $H_2{}^{17}O$ can be incorporated into the molecular-sieve framework.

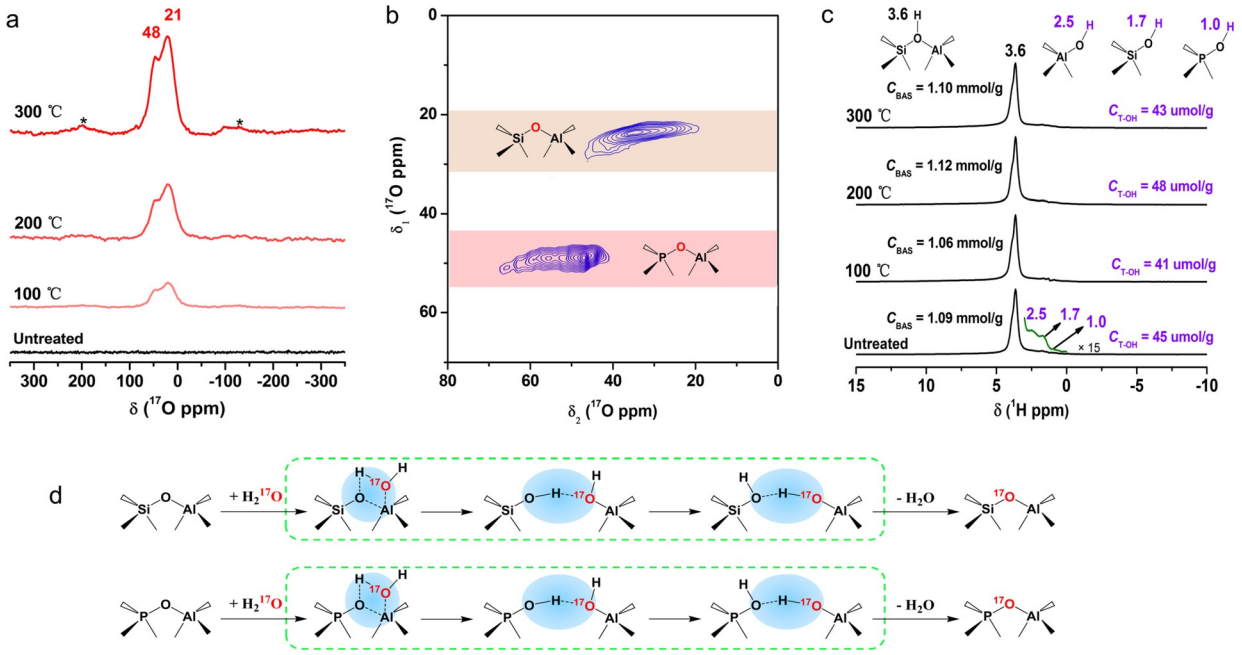

Figure 1. a) The ^{17}O MAS NMR spectra of $H_2{}^{17}O$ steamed SAPO-34 at 100 °C, 200 °C, and 300 °C, and the untreated sample for comparison. b) The 2D ^{17}O MQMAS NMR spectrum of $H_2{}^{17}O$ treated SAPO-34 at 300 °C. c) The ^{1}H MAS NMR spectra of $H_2{}^{17}O$ treated SAPO-34 at 100 °C, 200 °C, and 300 °C, and the untreated sample for comparison. Where T-OH presents the terminal hydroxy groups Al-OH, Si-OH, and P-OH. d) Schematic illustration of the proposed route for ^{17}O incorporation from $H_2{}^{17}O$ into the Si-O-Al (top) and P-O-Al (bottom) species and the substitution of original framework O atoms of molecular-sieve framework through reversible breaking and forming of T-O-T bonds. All the spectra in (a)–(c) were performed on a 4 mm H-X-Y triple resonance probe at room-temperature. Prior to NMR spectroscopy, all the $H_2{}^{17}O$ steamed samples and untreated sample were dehydrated at 300 °C for 2 h under vacuum. The asterisk (*) indicate spinning sidebands.

Encapsulating TMP and pyridine into CHA cavities under mild hydrothermal conditions

The CHA topology of SAPO-34 has the distinctive feature that all the T atoms in tetrahedral coordination state are located on the 8-MR window of framework. Therefore, the dynamic and reversible T-O-T bonds breaking and forming would cause the fast opening-closure behavior of 8-MR window, which may vary the transport of guest molecules and provide the accessibility for some bulky probe molecules, such as TMP and pyridine, whose kinetic diameters are much larger than the pore size of 8-MR window. Generally, due to the large size of TMP and pyridine, introduction of these bulky probe molecules into CHA cavities of SAPO-34 by encapsulation through the narrow 8-MR window has been believed as an impossible mission.[45]

A theoretical model was pre-constructed to predict the feasibility of TMP and pyridine molecules passing through intact and partially-opened 8-MR window connecting two adjacent cavities. The diffusion energy barriers calculated by periodic density functional theory (DFT) given in Figure 2 shows these bulky probe molecules passing through the intact 8-MR window is not feasible since the energy barriers are nearly 40 kcal mol^{-1}. Comparatively, a remarkably lowered diffusion energy barrier is predicted when one T–O bond of an 8-MR window is broken, with the energy barriers of 24.4 and 10.1 kcal mol^{-1} for the migration of TMP and pyridine, respectively. Meanwhile, when two opposite T–O bonds of an 8-MR window are broken simultaneously, only very low energy barriers (13.8 and 6.5 kcal mol^{-1} for TMP and pyridine, respectively) are required for passing through the 8-MR window. According to Kohen et al.[46] and Laaksonen et al.,[47] the diffusion energy barriers for CO_2 diffusion in Na-RHO and N_2 diffusion in Na-A, the examples of the small molecules passing through the 8-MR and cavity-type molecular sieves, are 15 and 7 kcal mol^{-1}, respectively. Therefore, TMP and pyridine encapsulation into CHA cavities of SAPO-34 through 8-MR window will become energetically feasible, if the 8-MR window is partially-opened. Another explanation is that the increase of temperature may cause some flexibility of the molecular-sieve pore opening,[48] however, when the temperature is considered for the model with intact 8-MR window, the diffusion energy barriers is still too high (45.5 kcal mol^{-1} at 100 °C and 41.1 kcal mol^{-1} at 300 °C) for the migration of these bulky probe molecules (Figure S5, take TMP as an example). In brief, the encapsulation of these bulky probe molecules into CHA cavities of SAPO-34 through the narrow 8-MR window is prohibited energetically even at high temperature, unless the 8-MR window is partially-opened with the breaking of T-O-T bonds. As being experimentally confirmed in this work, mild hydrothermal conditions can bring about dynamic and reversible T-O-T bonds breaking and forming, and thus the bulky probe molecules diffusion through 8-MR window will become energetically feasible. This encouraged us to conduct the hydrothermally-assisted encapsulation of the bulky probe

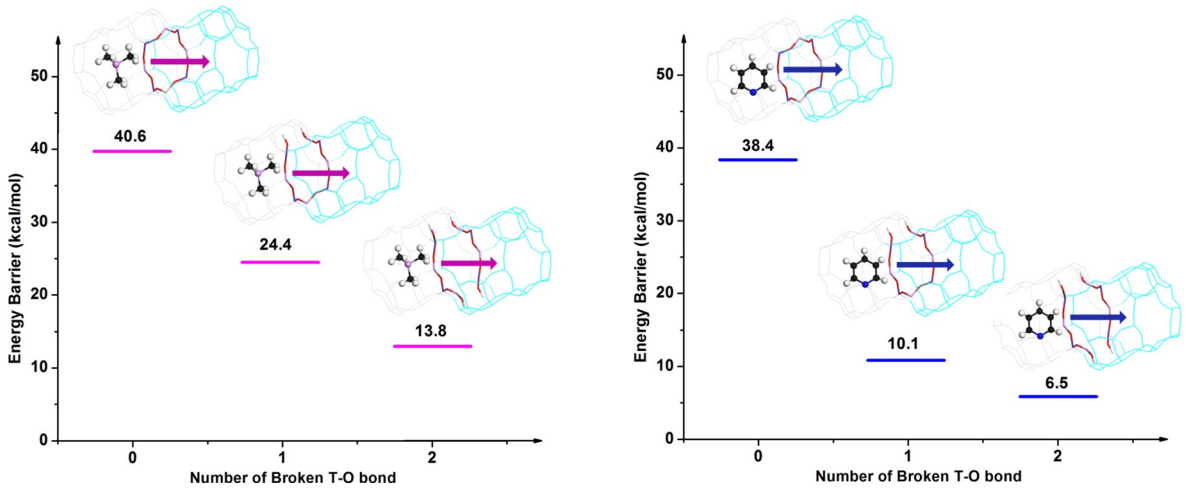

Figure 2. Calculated diffusion energy barriers (in kcal mol^{-1}) for TMP (left) and pyridine (right) passing through intact and partially opened 8-MR windows. Insets: schematic diffusion paths for TMP and pyridine. For the case of breaking two T–O bonds, the two broken bonds are in *para*-position of 8-MR window.

molecules into CHA cavities of SAPO-34 for the confirmation and consolidation of this water-induced dynamic and reversible process. Moreover, introducing these bulky probe molecules, TMP and pyridine, would be not only of great significance for exact identification and precise evaluation of the acidity in the 8-MR and cavity-type molecular sieves, but also very helpful for the achievement of shape selectivity in the SAPO-34-catalyzed reaction, such as MTO reaction.

A certain amount of water and TMP/pyridine were co-introduced into a tube where SAPO-34 was loaded and pre-dehydrated, then the tube was sealed and heated in the temperature range of 100–300 °C for 8 h. Upon adsorption of TMP/pyridine on Brønsted acid sites (BASs), the protonated form of TMP/pyridine, $[TMPH]^+$/$[PyH]^+$ ions will be formed and can be evidenced by ^{31}P and ^{1}H MAS NMR spectroscopy (Figure 3 a,c), from which the chemisorbed TMP/pyridine are quantified (Figure 3 b,d). For the case of no water co-introduction, due to the limitation of narrow 8-MR window, only the BASs located on the external surface of SAPO-34 ($\approx$1 % of the total BASs), are accessible and detectable with the chemisorption of TMP/pyridine. However, with the assistance of hydrothermal conditions, more BASs can be detected as indicated by the intensified signals of protonated TMP/pyridine, suggesting that these bulky probe molecules get into the CHA cavities of SAPO-34. Moreover, when the temperature for introducing TMP/pyridine in water vapor atmosphere goes up from 100 to 300 °C, the chemisorption of TMP and pyridine is largely improved due to the more intensified dynamic process of T-O-T bonds breaking and forming at enhanced temperature, as indicated by the ^{17}O incorporation results. Especially at 300 °C, 14.9 % and 41.8 % BASs are detected by the probing of TMP and pyridine, respectively. These results are in consistent with the FTIR spectra of pyridine-encapsulated SAPO-34 as evidenced that more pyridine can be encapsulated and adsorbed on BASs by the aid of hydrothermal condition at higher temperature (Figure S6). Based on the fluorescence characteristics of chemisorbed pyridine, confocal fluorescence provides more intuitive and visualized evidences for the encapsulation of bulky probe molecules into the CHA cavities of SAPO-34. As presented in Figure 3 e, the pure SAPO-34 shows no fluorescence signal. For the encapsulation at 300 °C, the higher molecular kinetic energy of pyridine at elevated temperature may promote this encapsulation process, while the promotion is very weak without water and thus only very little chemisorbed pyridine on external surface can be detected (Py-SAPO-34-300, Figure 3 f). However, for the hydrothermally-assisted pyridine encapsulation, the average pyridine penetration depth attains to ca. 0.8 um (Py-SAPO-34-300HT, Figure 3 g). These evidences directly and clearly reveal that the process of 8-MR window opening-closure under mild hydrothermal conditions greatly promotes the encapsulation of bulky probe molecules into CHA cavities of SAPO-34. The successful accommodation of TMP and pyridine in CHA cavities of SAPO-34 not only confirms the dynamic and reversible T-O-T bonds breaking and forming under mild hydrothermal conditions unambiguously, but also provided accessibility for some bulky probe molecules without deconstructing the molecular-sieve structure. An important work on revealing dynamic features of a working molecular sieve catalyst by the combination of synchrotron PDF analysis and in situ NMR spectroscopy has found a sudden change of Al–O bond lengths under industrially relevant operating conditions,[44] which is tally with our finding of the dynamic and reversible T-O-T bonds breaking and forming under mild hydrothermal conditions. Since many important zeolite/SAPO-catalyzed industrial catalytic processes are operated under hydrothermal condition with water vapor atmosphere and heating, the T-O-T bonds of these molecular sieves catalysts may also undergo a dynamic and reversible breaking and forming process under real catalytic reactions. Moreover, this dynamic process opens up a new strategy for introducing bulky probe molecules into small pore cavity-type molecular sieves for some important applications, such as acidity characterization and catalyst modification.

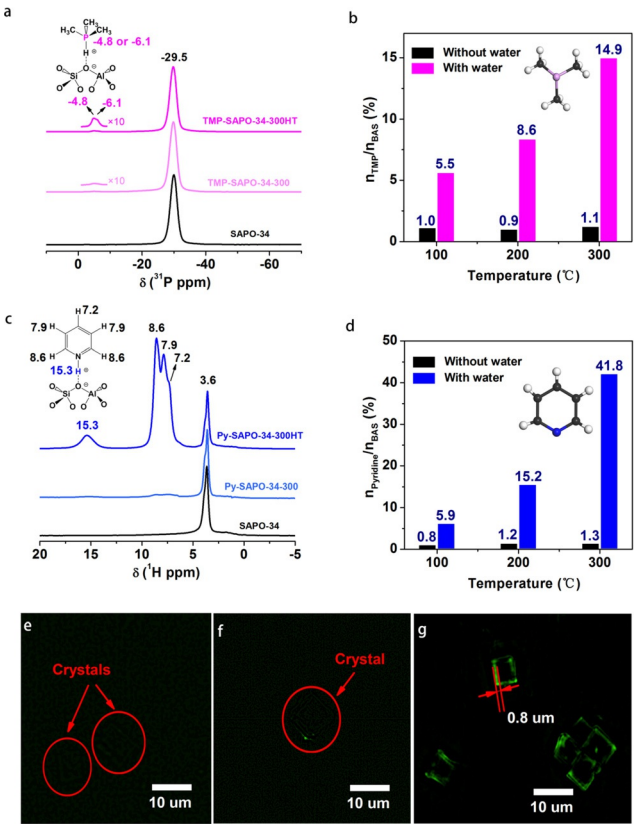

Figure 3. a) The ^{1}H decoupled ^{31}P MAS NMR spectra of SAPO-34, TMP-SAPO-34-300, and TMP-SAPO-34-300HT. TMP-SAPO-34-300: SAPO-34 with the encapsulation of TMP at 300 °C but without the aid of hydrothermal conditions. TMP-SAPO-34-300HT: SAPO-34 with the hydrothermally assisted encapsulation of TMP at 300 °C. Inset: schematic illustration of TMP adsorbed on BAS. b) The chemisorbed TMP at the temperature of 100–300 °C, which was quantified based on the intensity of the signals at −4.8 and −6.1 ppm (the signals of ^{31}P atoms in $[TMPH]^{+}$) in ^{31}P MAS NMR spectra in (a) and Figure S7. n_{TMP} (in mmol g^{-1}) is the amount of chemisorbed TMP per gram SAPO-34 (Table S1). n_{BAS} (1.09 mmol g^{-1}) is the Brønsted acid density of SAPO-34. c) The ^{1}H MAS NMR spectra of SAPO-34, Py-SAPO-34-300, and Py-SAPO-34-300HT. Py-SAPO-34-300: SAPO-34 with the encapsulation of pyridine at 300 °C but without the aid of hydrothermal conditions. Py-SAPO-34-300HT: SAPO-34 with the hydrothermally-assisted encapsulation of pyridine at 300 °C. Inset: schematic illustration of pyridine adsorbed on BAS. d) The chemisorbed pyridine at the temperature of 100–300 °C, which was quantified based on the intensity of the signal at 15.3 ppm (the signal of ^{1}H atoms in $[PyH]^{+}$) in ^{1}H MAS NMR spectra in (c) and Figure S8. $n_{Pyridine}$ (in mmol g^{-1}) is the amount of chemisorbed pyridine for per gram SAPO-34 (Table S2). All the experiments in (a) and (c) were performed on a 4 mm H-X-Y triple resonance probe. e)–g) The confocal fluorescence microscopy images of SAPO-34 (e), Py-SAPO-34—300 (f), and Py-SAPO-34-300HT (g). The confocal fluorescence microscopy measurements have been performed at the middle layer of crystals with an exciting laser at 405 nm (Figure S9 and S10).

Brønsted acidic sites identification for 8-MR SAPO molecular sieve

The dynamic and reversible T-O-T bonds breaking and forming in molecular sieve under mild hydrothermal conditions makes ship-in-a-bottle construction a realistic approach for multiple practical possibilities. Described here is a successful case of Brønsted acidic sites identification for 8-MR SAPO molecular sieves based on the successful encapsulation of TMP into CHA cavities of SAPO-34. The Brønsted acidity of molecular sieve is the key issue for their catalytic applications.[49] As sensitive basic probe molecule, TMP can give precise distinctions of acid sites location and strength,[39] while TMP probing is conventionally not suitable for SAPO-34 due to the limitation from narrow 8-MR window. Encapsulation of TMP into the CHA cavities of SAPO-34 based on the discovery of hydrothermally-assisted 8-MR opening-closure enables us to realize the fine and accurate identification of BASs for 8-MR microporous materials.

2D ^{1}H-^{31}P HETCOR (HETeronuclear CORrelation) NMR spectroscopy was conducted to present the interactions between TMP and the acid sites for BASs identification. As recorded in Figure 4a, A_1 and A_2 belong to the correlation peaks of ^{31}P and methyl ^{1}H in $[TMPH]^{+}$. Framework ^{31}P species exhibit correlations to TMP methyl ^{1}H at C and BAS proton at D. More importantly, the spatial interactions between ^{1}H and ^{31}P atoms present four cross-peaks from the signals at −4.8 and −6.1 ppm in the ^{31}P dimension and 5.8, 6.3, 6.7 and 7.3 ppm in the ^{1}H dimension (B_1, B_2, B_3 and B_4). In order to verify whether the multiple ^{1}H resonance signals come from ^{1}H-^{31}P J-coupling effect in $[TMPH]^{+}$,[50] ^{1}H spectroscopy with ^{31}P decoupling was performed and presented the remained four ^{1}H NMR signals of $[TMPH]^{+}$ (Figure S11), suggesting these cross-peaks are not resulted from ^{1}H-^{31}P J-coupling. Cross-peaks of B_1, B_2, B_3 and B_4 illustrate four BASs in SAPO-34. CHA crystal geometry contains one crystallographic T site with four nonequivalent O positions (O1, O2, O3 and O4 in Figure 4b). Si incorporation in the framework as T atoms gives rise to the negatively charged framework and positively charged BASs for compensation. Considering the SAPO-34 studied in this work presents has only one coordination state of Si(4Al) (Figure S4), the experimentally monitored four kinds of BASs should be originated from the bridging hydroxy groups (SiOHAl), whose protons are attached on the four nonequivalent O positions. Although the feasibility of the formation of BASs on the four nonequivalent O positions[51,52] and the jump of Brønsted proton on different O atoms at elevated temperature[44] have been theoretically predicated and experimentally observed, there still no experimental evidence for the direct identification of four different BASs in SAPO-34. Previous FTIR studies only suggested two kinds of bridging hydroxy groups in SAPO-34 from the absorbance peaks at ca. 3600 and 3627 cm^{-1}.[53] Herein, with the encapsulation of TMP to achieve sensitive probing, the slight differences of bridge hydroxy groups are revealed and fine identification is realized experimentally.

BASs location and strength are key issue for acid catalysis of zeolite/SAPO-catalyzed reactions. To evaluate the acidity of the BASs related to nonequivalent O positions, a quantitative internuclear spatial proximity between phosphorus atom in TMP and protons from BASs was measured by ^{1}H-{^{31}P} REDOR (Rotational Echo DOuble Resonance) experiment and the ^{1}H-^{31}P distances were extracted from REDOR

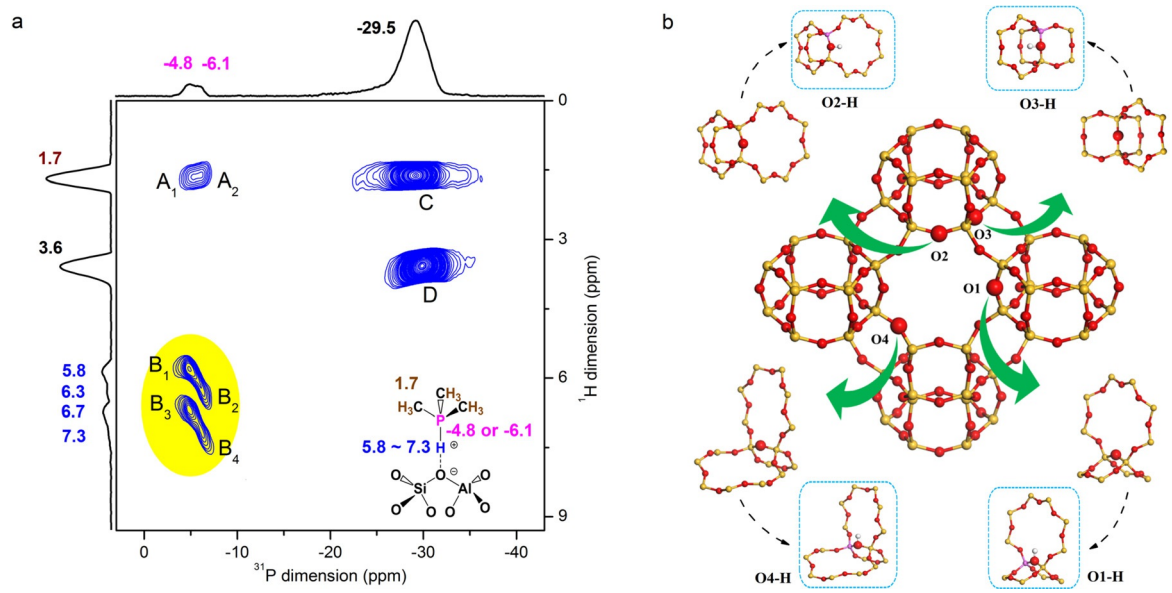

Figure 4. a) The 2D ^{1}H-^{31}P HETCOR NMR spectrum (performed on a 3.2 mm H-X-Y triple resonance probe) of TMP-SAPO-34–300HT with a contact time of 3 ms. The corresponding projections of ^{1}H and ^{31}P dimensions with chemical shifts (in ppm) are also shown. b) The CHA crystal geometry. Four O atoms are highlighted by enlargement. O atom locations, O1: two 4-MR and one 8-MR; O2: one 4-MR, one 6-MR and one 8-MR; O3: two 4-MR and one 6-MR; O4: one 4-MR and two 8-MR. The corresponding bridge hydroxy groups O1-H, O2-H, O3-H, and O4-H can be formed when a Si atom is located at an adjacent tetrahedral atom and a proton is attached to these O atoms for charge balance.

curves (Figure S12). The ^{1}H-^{31}P distances are 1.35, 1.42, 1.45 and 1.47 Å for four protons with signals at 5.8, 6.3, 6.7 and 7.3 ppm, respectively. The closer ^{1}H-^{31}P distance indicates the stronger acid strength of BAS,[54] and thus the acid strength order of $B_1 > B_2 > B_3 > B_4$ is revealed. Furthermore, adsorption energy of TMP (AE, defined as the energy difference between the adsorption state ($[TMPH]^{+}\cdots Zeo^{-}$) and the state before adsorption (H-form zeolite (H-Zeo) and probe molecules (TMP)), $AE = E_{[TMPH]^{+}\cdots Zeo^{-}} - E_{TMP} - E_{H\text{-}Zeo}$) is a reliable value for the evaluation of Brønsted acidity and a smaller AE value reflects the prone to protonation and thus a stronger Brønsted acid strength. The AE values for TMP adsorbed on bridge hydroxy groups O1-H, O2-H, O3-H and O4-H are predicted to be −21.85, −20.19, −19.97 and −18.68 kcal mol^{-1} (Table S3), indicating that the B_1, B_2, B_3 and B_4 in Figure 4a are originated from protons located on O1, O2, O3 and O4 respectively. The ^{1}H-^{31}P distances and the TMP adsorption energy are well confirmed for each other. This is the first time to realize the complete BASs identification of SAPO-34 molecular sieve and give exact acidic sequence of these bridge hydroxy groups. This knowledge would be of great significance for interpreting the acid catalysis of CHA-type molecular sieves as the important catalysts.

Shape-selective catalysis achievement with TMP/pyridine-encapsulation into molecular sieve

The discovery of dynamic and reversible T-O-T bonds breaking and forming in molecular sieve leads to the effective approach for bulky probe molecules encapsulation. Besides the sensitive identification of BASs, this extraordinary introduction of these bulky molecules into the CHA cavities of SAPO-34 also modifies the catalyst for shape selectivity in MTO reaction, the most successful industrial process for light olefins production from non-oil resources. It is known that, benefit from the mild acidity and shape-selective catalysis of 8-MR pore opening and super-cage structure, SAPO-34-catalyzed MTO reaction can achieve very high light olefins selectivity. However, efficient conversion of methanol for light olefins production with high selectivity cannot be realized from the beginning of the MTO reaction. Efficient MTO reaction follows indirect reaction pathway, consisting mainly of aromatics and cyclic carbenium ions as active intermediates of hydrocarbon-pool (HCP) mechanism.[55] The residence of the cyclic organics, polymethylbenzenyl compounds as reactive HCP species and polyaromatic hydrocarbons as coke species, in the CHA cavities of SAPO-34 imposes extra diffusion limitations on the generation and outflow of the higher hydrocarbon products, thereby enhancing the selectivity of the light olefins among the effluent products. MTO reaction typically encounters low initial light olefins selectivity due to insufficient diffusion limitations for depressing the higher hydrocarbons production over fresh catalyst without coke deposition. The consumption of methanol on coke deposition is a necessary strategy to obtain high selectivity of light olefins.[56,57] In this work, alternative and unique catalyst modification approach has been explored and shape-selective catalysis has been achieved (Figure 5a). Herein, two modified catalysts with encapsulation of TMP/pyridine, TMP-SAPO-34-300HT and Py-SAPO-34-200HT, were employed for improving the shape selectivity of MTO reaction. Firstly, mass transfer of hydrocarbon molecules in modified and fresh SAPO-34 were evaluated and calculated from the adsorption kinetics curves (Figure S13) measured by

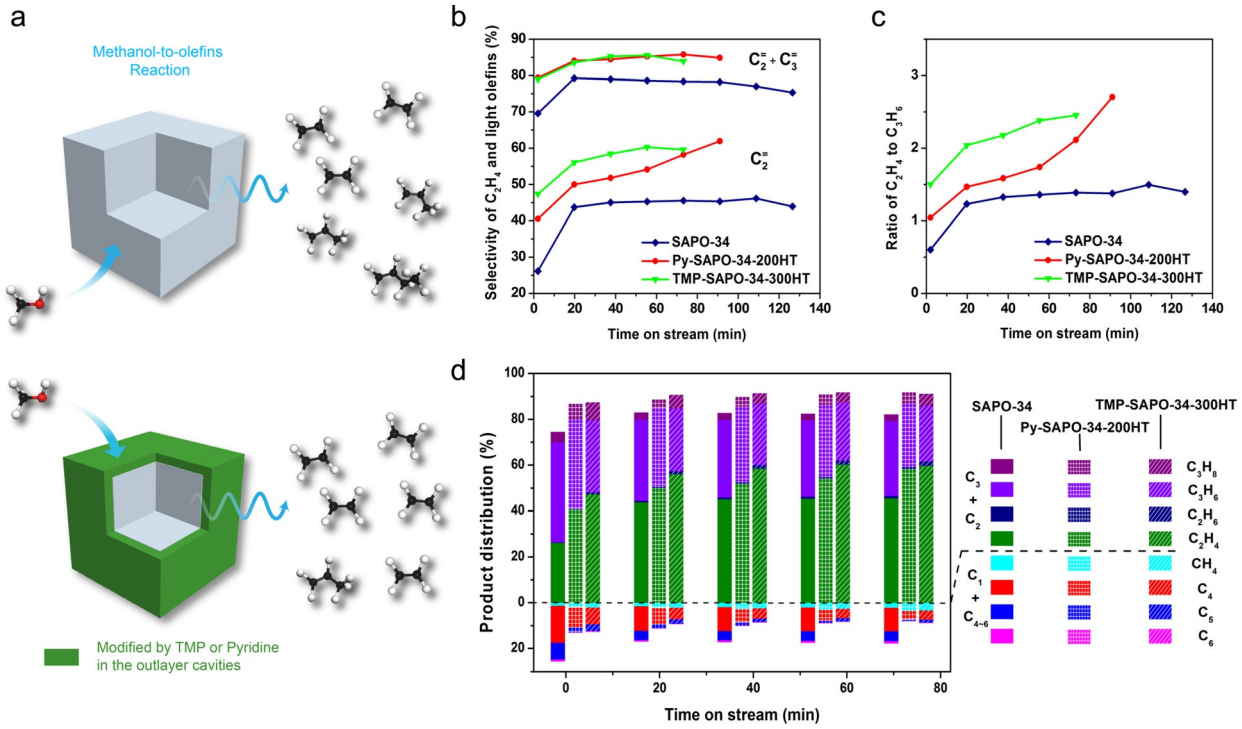

Figure 5. a) Schematic diagrams of the strategy for improving light olefins selectivity by imposing extra diffusion limitations via modifying the SAPO-34 catalyst with encapsulation of TMP or pyridine in the outerlayer cavities. b) The selectivity of ethene and light olefins of methanol conversion over fresh SAPO-34, Py-SAPO-34-200HT, and TMP-SAPO-34-300HT. Py-SAPO-34-200HT: SAPO-34 with the hydrothermally assisted encapsulation of pyridine at 200 °C. c) Ratio of ethene-to-propene. d) The product distribution. The MTO reaction was conducted at 475 °C with WHSV of methanol of 2 h^{-1}.

IGA (Intelligent Gravimetric Analyzer). Ethane and propane with very weak chemical adsorption on the catalysts were used as representing C_2 and C_3 probe molecules. As shown in Table S4, the diffusivity of ethane and propane in modified SAPO-34 is lower than that in fresh SAPO-34. At the same time, the diffusion activation energies (E_a) of ethane and propane increase with the encapsulation of bulky basic molecules in SAPO-34 (Table S5 and Figure S14). The introduced extra diffusion limitations, indicated by the decreased diffusivity and increased diffusion activation energies, would benefit shape selective production of light olefins. The catalytic performances of fresh SAPO-34 and TMP/pyridine-encapsulated SAPO-34 are presented and compared in Figure 5b. Light olefins selectivity is greatly enhanced over TMP/pyridine-encapsulated SAPO-34, especially at the initial period of MTO reaction. Proceeding the reaction for 2 min, 40% and 47% methanol is transferred to ethene over the two modified catalysts, Py-SAPO-34-200HT and TMP-SAPO-34-300HT respectively, while this value is only 26% for fresh SAPO-34. Meanwhile, the total selectivity of light olefins increases from 70% over fresh SAPO-34 to nearly 80% over TMP/pyridine-encapsulated SAPO-34, showing a remarkable enhancement in the selectivity of light olefins. Additionally, the ratio of ethene-to-propene also presents a notable increase (Figure 5c). The achievement of shape selectivity of MTO reaction is of great significance in improving the economics of this important industrial process.

Basic molecules entrapped in the CHA cavities in the outerlayer causes (Figure 3g) the loss of acid catalysis near the outer surface of SAPO-34. This makes the reaction to occur at the interior of the catalyst crystal and imposes extra diffusion restriction on higher hydrocarbons product outflow as effluent. The longer diffusion path and extra diffusion restriction significantly promoted hydrogen transfer reactions in modified catalysts (Figure S15), and consequently, HCP species, resulting from the hydrogen transfer reactions, can be accumulated rapidly (Figure S16). In contrast to fresh SAPO-34, shape selectivity is achieved for light olefins production over TMP/pyridine-encapsulated catalyst by moving the reaction environment from the outerlayer cavities to the interior cavities. By this modification strategy, the initial light olefins selectivity is improved by 10%, especially ethene selectivity increases by more than 22%. Since the extra diffusion restriction with TMP/pyridine encapsulation also affect the mass transfer of methanol and lower the accessibility of active sites with the reactant, the catalyst lifetime is slightly shortened over the modified catalysts (Figure S17), but this strategy is still worth being considered for improving the initial selectivity of light olefins when starting up a new MTO plant by using the modified catalyst with bulky molecules encapsulation in the outerlayer of catalysts. After the start-up step, the optimized operation with catalyst incomplete regeneration with retaining some organic in the catalyst can be performed in the continuous reaction-regeneration technology to ensure the efficient MTO reaction.[58]

Conclusion

We reveal a water-induced structural dynamic and reversible process in SAPO molecular sieves under mild hydrothermal conditions. This dynamic and reversible T-O-T bonds breaking and forming process was directly confirmed by the incorporation of ^{17}O atoms from $H_2{}^{17}O$ vapor into molecular-sieve framework and further consolidated by the encapsulation of bulky probe molecules, TMP and pyridine, into CHA cavities of SAPO-34 with hydrothermal assistance. The reversible hydrothermal stability of the framework and thus the feasibility of the introduction of bulky probe molecules larger than the pore size of the molecular sieve provide effective strategies for acidity identification and catalyst modification of molecular sieves, especially with small pore. The introduction of TMP into SAPO-34 molecular sieve presents the special host-guest interactions between BASs and probe molecules, which for the first time give very exact identification of four kinds of BASs originated from four nonequivalent O positions in framework. TMP/pyridine modification for MTO catalyst improves the light olefins selectivity as well as ethene-to-propene ratio, which can be used as a very efficient strategy for manipulating the shape selectivity of molecular sieve catalysts. These findings not only reveal the structural dynamic and reversible processes of the molecular sieves materials in the hydrothermal environment, but also provide an effective ship-in-a-bottle approach with great potential for wider range of applications.

Acknowledgements

This work was supported by the National Natural Science Foundation of China (No. 21972142, 21991092, 21991090, 91745109, 91545104), Liaoning Revitalization Talents Program (XLYC1807227), Key Research Program of Frontier Sciences, CAS (QYZDY-SSW-JSC024), International Partnership Program of CAS (12142KYSB20180007) and the Youth Innovation Promotion Association of CAS (2014165). We thank Prof. Bao-Lian Su for his kind suggestions.

Conflict of interest

The authors declare no conflict of interest.

Keywords: acidity · molecular sieves · MTO reaction · structural dynamic process · water

[1] P. Ball, *Nature* **2008**, *452*, 291 – 292.
[2] Z. Wu, J. Chen, Y. Wang, Y. Zhu, Y. Liu, B. Yao, Y. Zhang, M. Hu, *Natl. Sci. Rev.* **2018**, *5*, 452 – 454.
[3] J. Hu, Z. Cao, *Natl. Sci. Rev.* **2014**, *1*, 179 – 181.
[4] P. Wernet, D. Nordlund, U. Bergmann, M. Cavalleri, M. Odelius, H. Ogasawara, L. Å. Naslund, T. K. Hirsch, L. Ojamae, P. Glatzel, L. G. M. Pettersson, A. Nilsson, *Science* **2004**, *304*, 995 – 999.
[5] D. Su, *Natl. Sci. Rev.* **2015**, *2*, 138 – 139.
[6] Y. Ashida, K. Arashiba, K. Nakajima, Y. Nishibayashi, *Nature* **2019**, *568*, 536 – 540.
[7] H. Li, C. Qiu, S. Ren, Q. Dong, S. Zhang, F. Zhou, X. Liang, J. Wang, S. Li, M. Yu, *Science* **2020**, *367*, 667 – 671.
[8] Z. Jin, L. Wang, E. Zuidema, K. Mondal, M. Zhang, J. Zhang, C. Wang, X. Meng, H. Yang, C. Mesters, F. Xiao, *Science* **2020**, *367*, 193 – 197.
[9] C. S. Cundy, P. A. Cox, *Chem. Rev.* **2003**, *103*, 663 – 701.
[10] H. Chen, J. Wydra, X. Zhang, P. Lee, Z. Wang, W. Fan, M. Tsapatsis, *J. Am. Chem. Soc.* **2011**, *133*, 12390 – 12393.
[11] Database of Zeolite Structure. http://www.iza-structure.org/databases/.
[12] Z. Qin, K. A. Cychosz, G. Melinte, H. E. Siblani, J. P. Gilson, M. Thommes, C. Fernandez, S. Mintova, O. Ersen, V. Valtchev, *J. Am. Chem. Soc.* **2017**, *139*, 17273 – 17276.
[13] Z. Wang, Y. Jiang, O. Lafon, J. Trebosc, K. D. Kim, C. Stampfl, A. Baiker, J. P. Amoureux, J. Huang, *Nat. Commun.* **2016**, *7*, 13820.
[14] M. E. Davis, *Nature* **2002**, *417*, 813 – 821.
[15] G. Feng, P. Cheng, W. Yan, M. Boronat, X. Li, J. Su, J. Wang, Y. Li, A. Corma, R. Xu, J. Yu, *Science* **2016**, *351*, 1188 – 1191.
[16] I. I. Ivanova, Y. G. Kolyagin, I. A. Kasyanov, A. V. Yakimov, T. Bok, D. N. Zarubin, *Angew. Chem. Int. Ed.* **2017**, *56*, 15344 – 15347; *Angew. Chem.* **2017**, *129*, 15546 – 15549.
[17] H. Ma, Z. Tian, R. Xu, B. Wang, Y. Wei, L. Wang, Y. Xu, W. Zhang, L. Lin, *J. Am. Chem. Soc.* **2008**, *130*, 8120 – 8121.
[18] E. R. Cooper, C. D. Andrews, P. S. Wheatley, P. B. Webb, P. Wormald, R. E. Morris, *Nature* **2004**, *430*, 1012 – 1016.
[19] V. Kasneryk, M. Shamzhy, J. Zhou, Q. Yue, M. Mazur, A. Mayoral, Z. Luo, R. E. Morris, J. Cejka, M. Opanasenko, *Nat. Commun.* **2019**, *10*, 5129.
[20] S. Prodinger, M. A. Derewinski, A. Vjunov, S. D. Burton, I. Arslan, J. A. Lercher, *J. Am. Chem. Soc.* **2016**, *138*, 4408 – 4415.
[21] B. Arstad, A. Lind, J. H. Cavka, K. Thorshaug, D. Akporiaye, D. Wragg, H. Fjellvåg, A. Grønvold, T. Fuglerud, *Microporous Mesoporous Mater.* **2016**, *225*, 421 – 431.
[22] L. H. Ong, M. Dömök, R. Olindo, A. C. van Veen, J. A. Lercher, *Microporous Mesoporous Mater.* **2012**, *164*, 9 – 20.
[23] I. L. C. Buurmans, J. Ruiz-Martínez, W. V. Knowles, D. van der Beek, J. A. Bergwerff, E. T. C. Vogt, B. M. Weckhuysen, *Nat. Chem.* **2011**, *3*, 862 – 867.
[24] O. D. Mante, F. A. Agblevor, S. T. Oyama, R. McClung, *Appl. Catal. A* **2012**, *445 – 446*, 312 – 320.
[25] S. Eckstein, P. H. Hintermeier, R. Zhao, E. Barath, H. Shi, Y. Liu, J. A. Lercher, *Angew. Chem. Int. Ed.* **2019**, *58*, 3450 – 3455; *Angew. Chem.* **2019**, *131*, 3488 – 3493.
[26] M. Wang, N. R. Jaegers, M. S. Lee, C. Wan, J. Z. Hu, H. Shi, D. Mei, S. Burton, D. M. Camaioni, O. Y. Gutierrez, V. A. Glezakou, R. Rousseau, Y. Wang, J. A. Lercher, *J. Am. Chem. Soc.* **2019**, *141*, 3444 – 3455.
[27] L. Smith, A. K. Cheetham, R. E. Morris, L. Marchese, J. M. Thomas, P. A. Wright, J. Chen, *Science* **1996**, *271*, 799 – 802.
[28] Z. Li, J. M. Triguero, J. Yu, A. Corma, *J. Catal.* **2015**, *329*, 379 – 388.
[29] C. J. Heard, L. Grajciar, C. M. Rice, S. M. Pugh, P. Nachtigall, S. E. Ashbrook, R. E. Morriss, *Nat. Commun.* **2019**, *10*, 4690.
[30] S. M. Pugh, P. A. Wright, D. J. Law, N. Thompson, S. E. Ashbrook, *J. Am. Chem. Soc.* **2020**, *142*, 900 – 906.
[31] X. Zhao, J. Li, P. Tian, L. Wang, X. Li, S. Lin, X. Guo, Z. Liu, *ACS Catal.* **2019**, *9*, 3017 – 3025.
[32] Á. Ibarra, A. Veloso, J. Bilbao, J. M. Arandes, P. Castano, *Appl. Catal. B* **2016**, *182*, 336 – 346.
[33] K. De Wispelaere, C. S. Wondergem, B. Ensing, K. Hemelsoet, E. J. Meijer, B. M. Weckhuysen, V. Van Speybroeck, J. Ruiz-Martinez, *ACS Catal.* **2016**, *6*, 1991 – 2002.
[34] H. Deldari, *Appl. Catal. A* **2005**, *293*, 1 – 10.

[35] I. Yarulina, A. D. Chowdhury, F. Meirer, B. M. Weckhuysen, J. Gascon, *Nat. Catal.* **2018**, *1*, 398 – 411.
[36] S. S. Arora, D. L. S. Nieskens, A. Malek, A. Bhan, *Nat. Catal.* **2018**, *1*, 666 – 672.
[37] R. Zhang, N. Liu, Z. Lei, B. Chen, *Chem. Rev.* **2016**, *116*, 3658 – 3721.
[38] A. Wang, Y. Chen, E. D. Walter, N. M. Washton, D. Mei, T. Varga, W. Wang, J. Szanyi, Y. Wang, C. H. F. Peden, F. Gao, *Nat. Commun.* **2019**, *10*, 1137.
[39] A. Zheng, S. Liu, F. Deng, *Chem. Rev.* **2017**, *117*, 12475 – 12531.
[40] S. Yuan, J. Wang, Y. Duan, Y. Li, H. Jiao, *J. Mol. Catal. A* **2006**, *256*, 130 – 172.
[41] G. N. Kalantzopoulos, F. Lundvall, K. Thorshaug, A. Lind, P. Vajeeston, I. Dovgaliuk, B. Arstad, D. S. Wragg, H. Fjellvåg, *Chem. Mater.* **2020**, *32*, 1495 – 1505.
[42] L. Peng, Y. Liu, N. J. Kim, J. E. Readman, C. P. Grey, *Nat. Mater.* **2005**, *4*, 216 – 219.
[43] A. Sutrisno, B. E. G. Lucier, L. Zhang, L. Ding, Y. Chu, A. Zheng, Y. Huang, *J. Phys. Chem. C* **2018**, *122*, 7260 – 7277.
[44] G. N. Kalantzopoulos, F. Lundvall, S. Checchia, A. Lind, D. S. Wragg, H. Fjellvåg, B. Arstad, *ChemPhysChem* **2018**, *19*, 519 – 528.
[45] J. Liu, H. Xue, X. Huang, P. Wu, S. Huang, S. Liu, S. Shen, *Chin. J. Catal.* **2010**, *31*, 729 – 738.
[46] F. Coudert, D. Kohen, *Chem. Mater.* **2017**, *29*, 2724 – 2730.
[47] A. Mace, K. Laasonen, A. Laaksonen, *Phys. Chem. Chem. Phys.* **2014**, *16*, 166 – 172.
[48] A. Sartbaeva, S. A. Wells, M. M. J. Treacy, M. F. Thorpe, *Nat. Mater.* **2006**, *5*, 962 – 965.
[49] A. Zheng, S. Li, S. Liu, F. Deng, *Acc. Chem. Res.* **2016**, *49*, 655 – 663.
[50] H. Huo, L. Peng, Z. Gan, C. P. Grey, *J. Am. Chem. Soc.* **2012**, *134*, 9708 – 9720.
[51] C. Lo, B. L. Trout, *J. Catal.* **2004**, *227*, 77 – 89.
[52] Y. Jeanvoine, J. G. Angyan, G. Kresse, J. Hafner, *J. Phys. Chem. B* **1998**, *102*, 7307 – 7310.
[53] I. Halasz, B. Moden, A. Petushkov, J. Liang, M. Agarwal, *J. Phys. Chem. C* **2015**, *119*, 24046 – 24055.
[54] Y. Chu, Z. Yu, A. Zheng, H. Fang, H. Zhang, S. Huang, S. Liu, F. Deng, *J. Phys. Chem. C* **2011**, *115*, 7660 – 7667.
[55] J. Li, Y. Wei, J. Chen, S. Xu, P. Tian, X. Yang, B. Li, W. Wang, Z. Liu, *ACS Catal.* **2015**, *5*, 661 – 665.
[56] J. F. Haw, W. Song, D. M. Marcus, J. B. Nicholas, *Acc. Chem. Res.* **2003**, *36*, 317 – 326.
[57] J. Zhong, J. Han, Y. Wei, S. Xu, Y. He, Y. Zheng, M. Ye, X. Guo, C. Song, Z. Liu, *Chem. Commun.* **2018**, *54*, 3146 – 3149.
[58] P. Tian, Y. Wei, M. Ye, Z. Liu, *ACS Catal.* **2015**, *5*, 1922 – 1938.

Manuscript received: July 13, 2020
Accepted manuscript online: July 24, 2020
Version of record online: September 7, 2020

